Uwe Reisgen • Dietmar Drummer

Enhanced Material and Part Optimization and Process Intensification

Proceedings of the third International Joint Conference on
Enhanced Material and Part Optimization and Process Intensification EMPOrIA 2026
02nd and 03rd of June 2026, Aachen, Germany

Editors

Uwe Reisgen
RWTH Aachen University
Welding and Joining Institute
Germany

Dietmar Drummer
Friedrich-Alexander-Universität Erlangen-Nürnberg
Institute of Polymer Technology
Germany

Uwe Reisgen, Dietmar Drummer (eds.)

EMPOrIA 2026

Proceedings of the third International Joint Conference
on Enhanced Material and Part Optimization and
Process Intensification

Shaker Verlag
Düren 2026

Bibliographic information published by the Deutsche Nationalbibliothek
The Deutsche Nationalbibliothek lists this publication in the Deutsche Nationalbibliografie; detailed bibliographic data are available in the Internet at http://dnb.d-nb.de.

Shaker Verlag 2026

Print-ISBN 978-3-8191-0730-6
PDF-ISBN 978-3-8191-0670-5
https://doi.org/10.2370/9783819106705

Shaker Verlag GmbH • Am Langen Graben 15a • 52353 Düren
Phone: 0049/2421/99011-0 • Telefax: 0049/2421/99011-9
Internet: www.shaker.de • e-mail: info@shaker.de

Date: 30.03.2026

Influence of transient temperature on liquid metal embrittlement (LME) of Laser-DED brazed CuSn12Ni2 on 42CrMo4 investigated via 2D-quotient thermography

M. Troise[1*], K. Murthy[1], S. Olschok[1], U. Reisgen[1]

[1]RWTH Aachen University, Welding and Joining Institute - ISF, Pontstr. 49, 52062, AACHEN, GERMANY

*Corresponding author: E-mail: marcel.troise@isf.rwth-aachen.de, ORCID: 0009-0002-6836-7979

Abstract

The favorable tribological properties of bronze alloys such as CuSn12Ni2 allow for its use as brazing alloy for coating of tempered steel, mainly for components in tribological contact, including gears, pistons and bearings. Brazing via Laser-DED is an advanced coating method that allows for precise control of heat input and good mechanical properties. Liquid metal embrittlement (LME), a common defect in such joints, is strongly linked to transient temperature, which is difficult to measure due to the high temperature gradients and cooling rates. In this study, the thermal influence of the brazing process on liquid metal embrittlement is investigated using a specially developed 2D-quotient thermography setup. Considering influence of substrate temperature, process temperatures, and sample geometry, transient temperature is then correlated with LME crack length and frequency. The results demonstrate the viability of 2D-quotient thermography to investigate such processes and show a clear link between transient temperature and LME.

Keywords

Laser brazing, Laser material processing, Liquid Metal Embrittlement (LME)

1 Introduction

The application of bronze materials via brazing is a well-established industrial practice aimed at improving the tribological performance of steel components. It is widely utilized in sectors such as automotive engineering, aviation, and shipbuilding, particularly for components operating under tribological contact, including bearings, gears, pistons, and shafts. [1–8] Due to their favorable tribological and mechanical characteristics, tin bronzes such as CuSn12Ni2-c (CC484K) [9] and comparable alloys are especially suitable for these applications [1–3, 10–12]. Directed Energy Deposition (DED) via laser-powder or in this case, laser-wire deposition represents an effective brazing technique for joining dissimilar materials across a broad range of substrate materials. This process enables precise thermal control, facilitates the coating of complex geometries, and produces dense coatings with strong adhesion to the substrate [13–16], while also offering improved sustainability compared to conventional casting methods. Liquid metal embrittlement (LME), meaning the loss of ductility on a liquid-solid metal interface, has been recognized for decades in the context of brazing tin bronzes onto tempered steels . [17–20]. Liquid metal penetration (LMP) refers more specifically to the infiltration of the embrittling metal into the resulting cracks. In this work, LME is used as a collective term encompassing the observed cracking phenomena. The occurrence of LME leads to a deterioration of mechanical properties, particularly a reduction in the ductility of the base material [20]. Several mechanisms have been proposed to explain this type of metal-physical degradation. [20–25]. The likelihood of LME depends on various factors, including the specific material pairing of substrate and penetrant [20, 22]. In particular, copper and bronze alloys are known to induce LME in high-strength martensitic steels, thereby reducing their ductility [21]. Additional influencing factors include adequate interfacial contact, i.e., proper wetting of the substrate by the filler metal [22], the transient thermal conditions [23], and both residual and externally applied stresses within the substrate. These stresses may originate from prior manufacturing steps such as welding or from localized heat input during brazing. Furthermore, the initial microstructure of the substrate can also affect the susceptibility to LME [25]. To date, precise control of process parameters, including temperature gradients and strain distributions, has proven effective in mitigating LME [26]. It is well established that higher heat input increases the tendency for LME [19].

2 Aim of the Investigation

In this study, a comprehensive thermographic investigation of CuSn12Ni2-c onto 42CrMo4 using laser wire deposition has been conducted. The objective is to determine temperature distributions and cooling rates of the process by means of 2D quotient pyrometry. This method enables the characterization of the highly dynamic and otherwise difficult-to-measure process zone during laser brazing. These findings will be substantiated via analysis of the substrate temperature via classical thermography. The present study focuses on correlating transient temperature profiles with crack frequency and crack length. The goal is to identify and evaluate these parameters as additional factors influencing LME in this specific material system.

3 Materials and Experimental Details.

A schematic depiction of the laser-wire brazing setup is shown in Figure 1. The brazing setup uses a Trumpf Tru Disk 16002, with a 400 µm fibre diameter and optics with 200 mm collimation and 400 mm focal length. The focal position is set to 80 mm over the sample surface to archive a spot size of 7 mm. The CuSn12Ni2-c wire is fed into the center of the laser spot with a drag angle of 45°. The process is shielded using 15 l/min argon 4.6 gas. The deposition strategy involves brazing of a spiral shape, initiated from the center of the specimen and progressing outward with a layer overlap of 50% and a layer width of 8 mm. This is followed by the completion of an additional circle, ensuring coverage of the specimen. The spiral is created by rotating the workpiece while moving the laser brazing head outwards. The relative brazing speed remains constant during the deposition process.

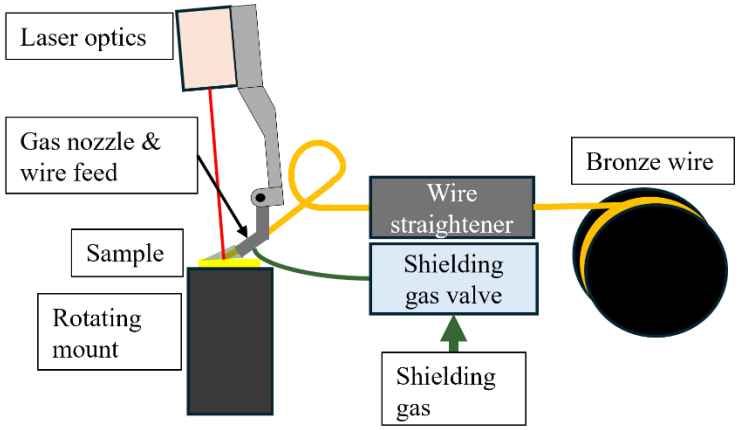

Figure 1: Schematic depiction of the laser-wire brazing setup

Two parameter sets were selected for brazing, shown in **Table 1**. A lower deposition rate parameter, which tends to cause more cracks, and a high deposition rate parameter, which causes fewer cracks, as preliminary investigations have shown. All other parameters remained constant and are described below.

Table 1: Laser brazing parameters

Parameter	Unit	Sample 1	Sample 2
Laser power	W	3500	3600
Brazing speed	mm/s	16	16
Energy per unit length	J/mm	220	225
Wire feed	mm/s	87	75
Deposition rate	g/min	45	41

The 42CrMo4 samples were machined to Ø 114 x 18 mm discs. Brazing filler metal was CuSn12Ni2, diameter d = 1 mm. Material composition of the materials used are listed in Table 2. Samples are degreased and coated in Castolin Flux 18 before deposition.

Table 2: OES analysis of base materials and filler wire composition according to [27] in m%

Material	C [m%]	Si [m%]	Mn [m%]	P [m%]	S [m%]	Cr [m%]	Mo [m%]
42CrMo4	0.387	0.281	0.822	0.0078	0.0161	1.06	0.184
Material	Ni [m%]	Sn [m%]	Zn [m%]	Pb [m%]	Fe [m%]	Mn [m%]	P [m%]
CuSn12Ni2	1.5-2.4	11.3-13.0	≤0.3	≤0.2	≤0.15	≤0.1	≤0.05

An Optris Xi410 LT ETH thermal camera was used to determine substrate temperature i.e. sample temperature. The measurement data was referenced using data from thermocouple measurements to correct for the emission coefficient, which changes with temperature. A specially built 2D-quotient thermography camera, designed by University of Stuttgart, Institut für Strahlwerkzeuge – ISFW, was used to analyze process temperatures, as detailed in the literature [28].

4 Results and Discussion

The as-deposited, laser-brazed samples are presented in Figure 2 a) and b). The darker appearance of sample B indicates elevated deposition temperatures, as evidenced by the more pronounced surface oxidation. While deposition rate and laser power vary between the two samples, shielding gas flow was maintained.

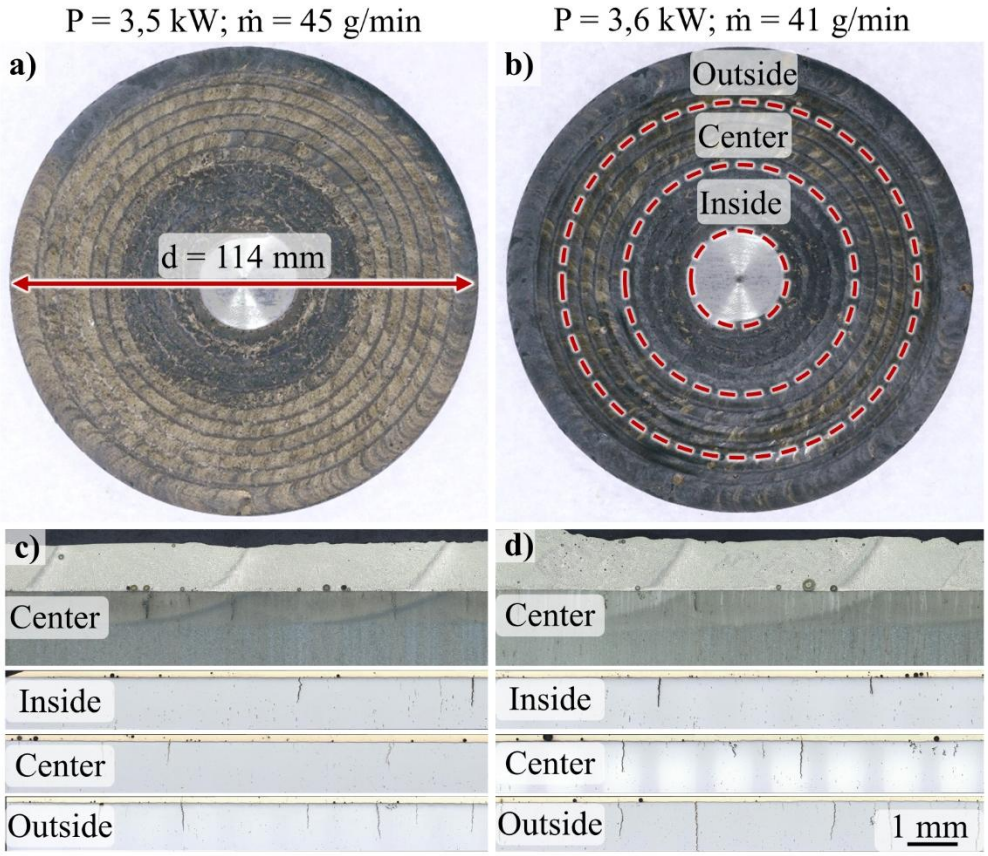

Figure 2: Images of the laser brazed samples and cross sections of the analyzed sample sections

The deposition strategy is discernible in the images. Upon completion of the spiral path, an additional rotation was performed without translational movement of the laser head, ensuring full coverage of the sample geometry, while the center of the samples remains uncoated. For cross-

sectional analysis as well as characterization of LME cracks size and distribution, the samples were subdivided into the regions “inside,” “center,” and “outside,”. Figure 2 c) and d) shows exemplary cross sections of the sectioned sample, as indicated in Figure 2 b). As deposition rate varies only slightly between the two parameter sets the layer thickness is similar. The top images in Figure 2 show an overview of the deposited coatings. The width of the individual layers is discernible. The structure is dense but shows some porosity. Porosity in such coatings is seen in the literature and can be optimized by means of optimizing deposition rate, laser power and gas shielding [2, 3]. Below the coating, the substrate HAZ can be seen. Hardness is H = 400 HV0,5 right below the coating interface and linearly decreases to H = 250 HV0,5, which is the base material hardness, at around 1,5 mm distance from the interface. The three cross sections below show polished sections that were used to measure the crack length and distribution. Crack quantification was performed based on ten cross-sections per sample position, as indicated in Figure 2 b). As the standard relevant to laser brazing (ISO 18279) does not specify a minimum crack size, crack evaluation was conducted in accordance with DIN EN ISO 13919-1. Accordingly, features requiring magnification greater than 500× for unambiguous identification were excluded from the analysis, resulting in a minimum detectable crack length of approximately 20 µm.

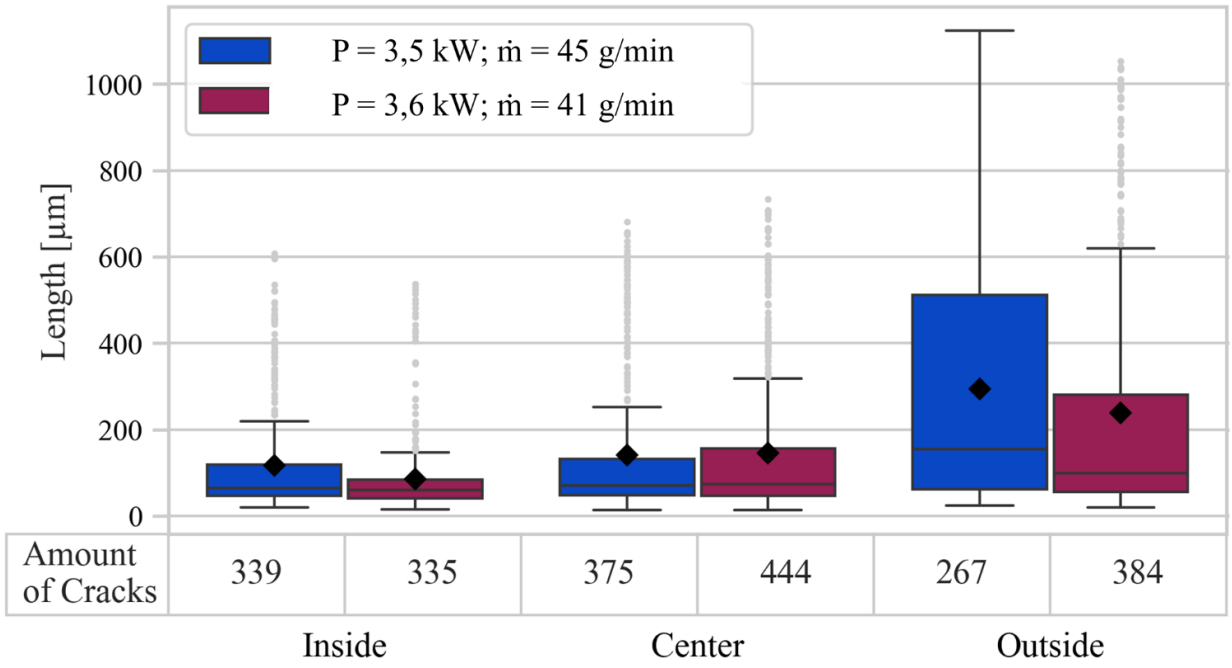

Figure 3: Boxplots of crack length and distribution

Figure 3 shows the crack length distributions for both samples across the inner, center, and outer regions. In the inner region, the median crack lengths differ only slightly (~5 µm), with values of approximately 64 µm for the lower energy input and 59.4 µm for the higher energy input. Furthermore, the interquartile ranges are comparatively small for both cases and the total amount of cracks is roughly the same. In the center region, the median values remain similar, differing by only ~3 µm, with slightly higher crack lengths overall. However, the interquartile ranges increase, particularly for the P = 3,6 kW sample, which also exhibits a greater number of cracks across most size ranges. In the outer region, more pronounced differences are observed. The median crack

length for the lower energy input (≈154 µm) is significantly higher than that of the higher energy input (≈99.5 µm). Additionally, the interquartile range is substantially larger. While the higher energy input results in more cracks at smaller sizes (<200 µm), the lower energy input shows a higher frequency of cracks in the intermediate range (~200–700 µm). Overall, the higher energy input tends to produce more small cracks, and therefore more cracks in total. Whereas both conditions exhibit comparable maximum crack lengths and similar distribution characteristics at the extremes.

Strain-, stress-, and temperature-induced LME effects are altered in the outer regions of the samples, as can be seen by the greatly increased crack sizes, but a decrease in number of cracks. This may result from increased substrate temperature due to preceding laser process [19], as well as altered strain and stress conditions near the sample edge [29–31]. Since both samples share identical geometry, the higher median crack amount across center and outside indicates a predominantly thermal origin. Overall, a clear trend is observed toward higher crack density and longer crack growth as process time progresses and temperature increases. Heat accumulation may delay the solidification of the molten metal, thereby extending liquid metal exposure time. These hypotheses are explored in the following sections.

Figure 4 shows the substrate temperatures of both samples, measured at 12 equidistant points. The measurement range of the camera was calibrated against thermocouple data to correct for the temperature-dependent variation in the emissivity coefficient. Table 3 shows a moving average with a window size of 40 data points, corresponding to a time interval of 0.5 seconds. This temperature can be considered representative of the substrate temperature right before the corresponding brazing layer is applied.

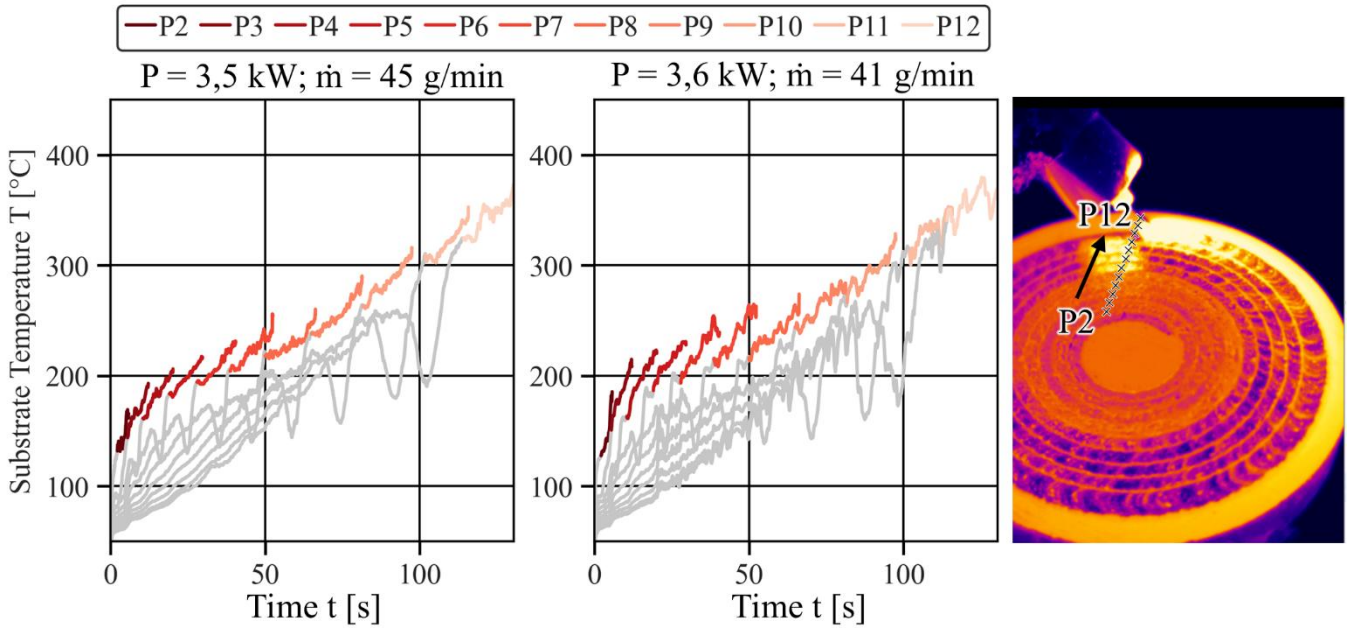

Figure 4: Substrate temperatures over time based on 12 measurement points

The minima observed prior to the selected measurement intervals result from process shadowing caused by the wire, enabling precise temporal identification of the relevant regions. In the process with lower energy input, the substrate temperature increases on average by 9.04% between successive layers, while for the higher energy input spiral, the increase is 8.26%. In general, the difference in preheating temperature between the two spirals decreases with increasing number of layers, i.e. in the progressing brazing process. Starting from around 9% and decreasing to less than 1% in the outside layers.

Table 3: Calculated substrate temperatures at selected points

Point	Section	P = 3,5 kW	P = 3,6 kW	Difference in %
Layer 2	Inside	145,2	157,8	8,68 %
Layer 4	Inside	183,5	192,4	4,85 %
Layer 6	Center	208,1	219,1	5,29 %
Layer 8	Center	228,9	233,7	2,1 %
Layer 10	Outside	284,9	285,8	0,32 %
Layer 12	Outside	343,2	345,4	0,64 %

In the inside regions, cracking behaves very much the same between the two samples. The 5-10% difference in substrate temperature in the inner layers does not amount to a difference in cracking behavior. In the later stages, temperature differences equalize and diminish completely in the outside regions. Nonetheless, here the number of cracks differs between hotter and colder process, suggesting little influence of the substrate temperature itself on LME phenomena in this case. Sample temperature is T = 280 °C or higher in both samples in the outside regions. Since both Samples exhibit less, but much longer cracks in those areas, having reached this temperature might be one of the conditions necessary for this behavior.

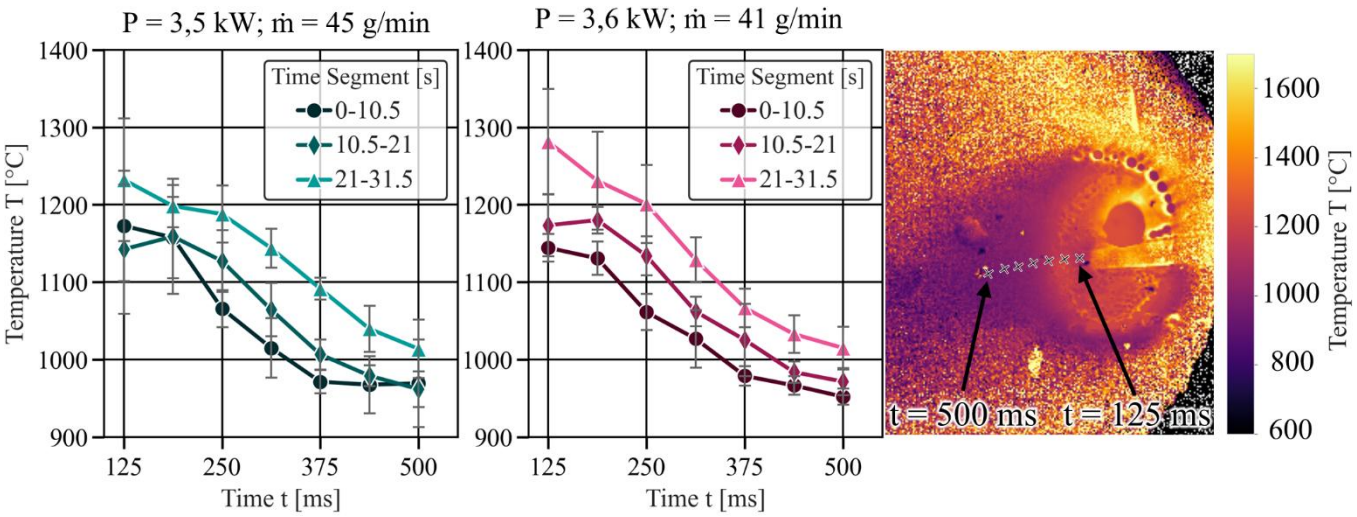

Figure 5: Quotient pyrography measurement of the process temperatures.

Figure 5 shows the process temperatures over time in selected time segments. Peak temperature at around 2 mm distance from the center of the laser spot is around T = 1150 °C in the early time segment in both processes. The cooling rate is at around 550 °C/s, meaning that T_{solid} = 830 °C is

reached from peak temperature after about 0.62 s. In later stages of the process, the peak temperature rises as the substrate warms up. Yet the cooling rate remains similar. Cooling down to solidus therefore takes longer since peak temperature has increased, causing a longer liquid-solid contact time and more time for cracks to develop and grow, explaining the higher number of cracks in the center regions. Especially in the later segments, temperatures of the P = 3,6 kW sample increase more. On average that process is slightly hotter on most points of measurement, resulting in increased crack amount in the hotter samples in those regions. In the outside region, the number of cracks reduces again, instead many cracks become much larger, as shown in Figure 3. Since the peak temperatures of the higher energy process are reached by the lower energy process only in later stages, a critical temperature for the development of fewer but lager cracks cannot be determined, inferring that the spatial location on the sample outside, where strain can develop more easily due to less support of surrounding material may likely be the reason for this behavior, rather than transient temperature alone. Furthermore, differences in crack morphology between segments may be attributed to variations in local stress states. Lower compressive stresses in the outer regions may facilitate grain boundary opening, thereby promoting the formation of longer LME cracks. Previous studies have demonstrated the significant influence of the stress field on LME behavior, indicating that a more detailed characterization of the stress and strain states during processing is necessary to establish accurate correlations between crack formation and spatial location [29–31].

5 Summary

Two-dimensional quotient thermography has proven to be a suitable method for measuring and characterizing the complex thermal conditions present during laser brazing. In combination with conventional thermography, it enables a nearly comprehensive thermal analysis of the process. Transient temperature has a pronounced effect on crack formation. Increased occurrence of LME cracks and lager crack sizes correlate with increased substrate as well as process temperatures, indicating that controlled cooling phases may represent an effective strategy for mitigating LME cracking. Although reduced heat dissipation in an already preheated workpiece should affect crack formation, it does not account for the difference in crack formation between the lower energy and higher energy sample, suggesting increased process temperatures to be the main influence. The observed increase in crack length toward the outer regions is not attributable to extended diffusion times resulting from prolonged dwell times above the solidus temperature, as the hotter process reaches higher temperatures much earlier in the process, yet behaves similarly with regards to the spatial locations of the longer cracks, suggesting that local stress fields and strain distribution in the outside regions of the sample to be the main influence.

Acknowledgements

The presented investigations were carried out at RWTH Aachen University within the framework of the Collaborative Research Centre SFB1120 236616214 “Bauteilpräzision durch Beherrschung von Schmelze und Erstarrung in Produktionsprozessen” and funded by the Deutsche

Forschungsgemeinschaft e.V. (DFG, German Research Foundation). The sponsorship and support is gratefully acknowledged.

Conflict of Interest

The author declares no conflict of interest.

Data Availability Statement

The data that supports the findings of this study are available at http://hdl.handle.net/21.11102/01338aea-287e-4ac3-a88f-19d7d45403db upon request.

References

[1] P. K. Hu *et al., Influence of Ni content on electrochemical corrosion and tribological behavior of Cu-10Sn coatings by laser cladding*, Materials Today Communications, **2024**

[2] S. Raghavendra *et al., Process enhancements and wear evaluation of directed energy deposited bronze: Implications for reducing bronze in worm gear manufacturing*, Journal of Materials Research and Technology, **2025.**

[3] S. Raghavendra, *et al, Development of DED Process Parameters for Deposition of Bronze and Evaluation of Its Wear Properties under Dry Sliding Conditions,* Procedia Structural Integrity, **2024.**

[4] M.V.S. *Babu et al. Review of Journal Bearing Materials and Current Trends*, American Journal of Materials Science and Technology, **2015**.

[5] V. Fontanari *et al., Tribological behavior of the bronze–steel pair for worm gearing,* Wear, **2013.**

[6] V. Mastan *et al.*, *study of Friction and Wear on Journal Bearings,* International Refereed Journal of Engineering and Science (IRJES), **2012**.

[7] Biryukov, V. P. *et al*., *Laser Cladding of Copper Alloys on Steel* Phys. Atom. Nuclei **2019.**

[8] Le Wan, *et al., Annular laser cladding of CuPb10Sn10 copper alloy for high-quality anti-friction coating on 42CrMo steel surface*, Optics & Laser Technology, **2023**.

[9] DIN EN 1982, *Kupfer und Kupferlegierungen –Blockmetalle und Gussstücke*; Deutsche Fassung EN 1982:2024

[10] F. Rippa*, et al., Bronze-on-steel deposition with blue light high-speed Laser Cladding and IR Laser Cladding properties and differences*, Procedia CIRP 124 **2024.**

[11] Jie Chen, *et al., Influence mechanism of process parameters on the interfacial characterization of selective laser melting 316L/CuSn10*, Materials Science and Engineering: A **2020**.

[12] S. Raghavendra *et al., Wear and material characterization of CuSn10 additively manufactured using directed energy deposition,* Additive Manufacturing Letters 2023

[13] V. P. Biryukov *et al, Laser Cladding of Copper Alloys on Steel*, Phys. Atom. Nuclei, **2019.**

[14] H. Hügel und T. Graf, *Laser in der Fertigung: Strahlquellen, Systeme, Fertigungsverfahren,* 2. Aufl. Wiesbaden: Vieweg + Teubner, **2009**.

[15] L. Zhu *et al., Recent research and development status of laser cladding: A review*, Optics & Laser Technology, **2021**.

[16] A. S. Bolokang *et al., Laser cladding—a modern joining technique*, Advanced Welding and Deforming **2021**.

[17] M. H. Razmpoosh *et al., Atomic-scale Investigation of Liquid-Metal-Embrittlement Crack-path: Revealing Mechanism and Role of Grain Boundary Chemistry,* Acta Materialia, **2021**.

[18] M. H. Razmpoosh *et al., Pathway to understand liquid metal embrittlement (LME) in Fe-Zn couple: From fundamentals toward application,* Progress in Materials Science, **2021**.

[19] J. E. Norkett *et al., A Review of Liquid Metal Embrittlement: Cracking Open the Disparate Mechanisms,* Metall Mater Trans **2021**.

[20] M. G. Nicholas and C. F. Old, *Liquid metal embrittlement*, J Mater Sci,**1979**.

[21] S. P. Lynch, *Failures of structures and components by metal-induced embrittlement*, Stress Corrosion Cracking Theory and Practice **2011**.

[22] P. J. Fernandes and D. R. Jones, *Specificity in liquid metal induced embrittlement: Specificity in liquid metal induced embrittlement*, Engineering Failure Analysis, **1996**.

[23] C. F. Old, *Liquid metal embrittlement of nuclear materials,* Journal of Nuclear Materials,**1980**

[25] W. F. Savage, *et al., Intergranular attack of steel by molten copper,* Welding Research Supplement, **1978**.

[26] S. Chen, *et al., Interfacial ferrite band formation to suppress intergranular liquid copper penetration of solid steel,* Journal of Alloys and Compounds, **2019**.

[28] U. Reisgen, et al., *Temporally and spatially controlled temperature fields during material processing with the electron beam*, DVS Verl, RWTH **2021.**

[29] M. I. Chaevskii, et al., *Role of stresses in accelerating the penetration of liquid into solid metals*, Mater Sci, **1972**.

[30] C. DiGiovanni *et al, Liquid metal embrittlement transport mechanism in the Fe/Zn system: Stress-assisted diffusion,* Materialia, **2021**.

[31] K. Yang, *et al, The Identification of a New Liquid Metal Embrittlement (LME) Type in Resistance Spot Welding of Advanced High-Strength Steels on Reduced Flange Widths*, metals **2023**.